ARTICLE

An arginine residue in the outer segment of hASIC1a TM1 affects both proton affinity and channel desensitization

Zhuyuan Chen[1], Georg Kuenze[2,3,5], Jens Meiler[2,3,4,5], and Cecilia M. Canessa[1,6]

Acid-sensing ion channels (ASICs) respond to changes in pH in the central and peripheral nervous systems and participate in synaptic plasticity and pain perception. Understanding the proton-mediated gating mechanism remains elusive despite the of their structures in various conformational states. We report here that R64, an arginine located in the outer segment of the first transmembrane domain of all three isoforms of mammalian ASICs, markedly impacts the apparent proton affinity of activation and the degree of desensitization from the open and preopen states. Rosetta calculations of free energy changes predict that substitutions of R64 in hASIC1a by aromatic residues destabilize the closed conformation while stabilizing the open conformation. Accordingly, F64 enhances the efficacy of proton-mediated gating of hASIC1a, which increases the apparent pH_{50} and facilitates channel opening when only one or two subunits are activated. F64 also lengthens the duration of opening events, thus keeping channels open for extended periods of time and diminishing low pH-induced desensitization. Our results indicate that activation of a proton sensor(s) with pH_{50} equal to or greater than pH 7.2–7.1 opens F64hASIC1a, whereas it induces steady-state desensitization in wildtype channels due to the high energy of activation imposed by R64, which prevents opening of the pore. Together, these findings suggest that activation of a high-affinity proton-sensor(s) and a common gating mechanism may mediate the processes of activation and steady-state desensitization of hASIC1a.

Introduction

Acid-sensing ion channels (ASICs) are proton-activated cation channels expressed broadly in neurons of the central and peripheral nervous systems. They contribute to important physiological processes such as nociception (Deval and Lingueglia, 2015; Bohlen et al., 2011), modulation of synaptic signaling (Wemmie et al., 2002; Kreple et al., 2014; González-Inchauspe et al., 2017), generation of fear (Du et al., 2017; Taugher et al., 2017), and addiction-related behaviors (Kreple, et al., 2014). ASIC1a is the most abundant and broadly expressed isoform in the brain; inactivation by knock-out of the gene in mouse brain eliminates transient proton-induced currents in neurons (Wemmie et al., 2002).

ASICs are made of three identical or homologous pore-forming subunits; each subunit has a large extracellular domain (ECD) folded in a structure resembling a hand with subdomains referred as palm, thumb, finger, and knuckle. The ECD is connected to two transmembrane helices, TM1 and TM2, and short intracellular N and C termini. TM2 and a reentrant loop formed by the N terminus (Yoder and Gouaux, 2020) make

most of the ion conduction pathway in the cytoplasmic side of the pore. The interface between the thumb and the finger subdomains contains a cluster of negatively charged residues called the "acidic pocket." Crystal and cryo-EM structures of chicken ASIC in various conformational states have demonstrated that displacement of the thumb with collapse of the acidic pocket are part of the gating mechanism initiated by protons (Jasti et al., 2007; Baconguis et al., 2014; Yoder et al., 2018). Functional studies using various experimental approaches have also documented movement of the thumb during gating (Paukert et al., 2008; Ramaswamy et al., 2013; Krauson and Carattino, 2016; Vullo et al., 2017). However, the roles of the negatively charged residues in the acidic pocket driving gating and in particular collapse of the acidic pocket have remained inconclusive. Reports of the consequences of neutralizing negatively charged residues in the pocket range from elimination of currents (Ramaswamy et al., 2013), to shifts of the apparent pH_{50} of activation (pH_{50a}) to more acidic values (Jasti et al., 2007; Li et al., 2009; Vullo et al., 2017; Yoder and

[1]Department of Basic Sciences, Tsinghua University School of Medicine, Beijing, China; [2]Department of Chemistry, Vanderbilt University, Nashville, TN; [3]Center for Structural Biology, Vanderbilt University, Nashville, TN; [4]Department of Pharmacology, Vanderbilt University, Nashville, TN; [5]Institute for Drug Discovery, Leipzig University, Leipzig, Germany; [6]Cellular and Molecular Physiology, Yale University, New Haven, CT.

Correspondence to Cecilia M. Canessa: ccanessa@tsinghua.edu.cn.

Gouaux, 2018), to no effect (Krauson and Carattino, 2016). Together, these results have raised the possibility that contraction of the pocket is not caused directly by protons binding to residues in the acidic pocket, but rather it may represent an allosteric conformational change initiated when protons bind elsewhere in the ECD (Rook et al., 2020a), though the nature and location of those residues have not been yet determined.

Another feature of hASIC1a is complete desensitization from the open and preopen states. Desensitization from the open state manifests as decay of currents to the zero level in the continued presence of protons, whereas from the preopen state, also referred as steady-state desensitization (SSD), channels desensitize before opening. SSD occurs at proton concentrations much lower than those required for open state desensitization. Desensitization shapes the time course of the currents and is functionally important to protect neurons from excessive depolarization when exposed to prolonged acidic conditions (Sherwood and Askwith, 2009; Chassagnon et al., 2017).

The mechanism of desensitization of ASIC1a is also not fully understood yet. Mutations in various domains of the channel accelerate desensitization, but in almost all instances the underlying mechanism has not been elucidated. Early reports, before any structural information of ASICs was available, showed that the β1-β2 (Li et al., 2010a) and β11-β12 (Li et al., 2010b) linkers alter the rate of desensitization, pointing to a possible role in the desensitization mechanism. Subsequently, it was observed that the structure of the β11-β12 linker in resting (PDB accession nos. 5WKV, 6AVE) and open (4NTW) conformations was different from those in high and low pH desensitized states (3IJ4, 2QTS, 6VTK). Specifically, in the desensitized states, there is a change in the shape of the β11-β12 linker, and the residues L414 and N415 undergo a 180° rotation, reorientating the side chain of L414 toward the central vestibule. This conformational difference led to the proposal that reorganization of the β11-β12 linker enables desensitization upon exposure to protons: it serves as a molecular clutch that disengages the upper from the lower half of the ECD (Yoder et al., 2018; Fig. S1). The functional significance of the linker isomerization has been recently confirmed (Wu et al., 2019; Rook et al., 2020b), though it remains to be determined what the trigger of the isomerization is.

In this study, we take advantage of ASIC channels with high amino acid sequence identity but markedly different functional properties, lamprey and human ASIC1a, to identify elements in the channel protein that are important in determining the apparent pH_{50a} and the gating steps that lead to opening and desensitization. We present evidence that residue R64 in the outer segment of TM1 plays crucial roles in both of these processes.

Materials and methods
Homology modeling of hASIC1a and lASIC
Structural models of hASIC1a (residues L41-E456; Uniprot accession no. P78348) and lASIC (residues V43-E459; Uniprot accession no. Q1XA79) in closed, desensitized, and open states were developed by homology modeling using the protein structure prediction software Rosetta (version 3.11; Leman et al.,

2020). The crystal structure of chicken ASIC1 (cASIC1; Uniprot accession no. Q1XA76) determined at high pH (PDB accession no. 5WKV; Yoder et al., 2018) served as the template for the closed state model. The structures of cASIC1 determined at low pH (PDB accession no. 4NYK; Gonzales et al., 2009) or in complex with the MitTx snake toxin at pH 5.5 (PDB accession no. 4NTW; Baconguis et al., 2014) were used for modeling the desensitized or open state structure, respectively. Prior to homology modeling, missing loop residues in the open state structure of cASIC1 (D297, S298) were added with RosettaRemodel (Huang et al., 2011) guided by PSIPRED (Jones, 1999) secondary structure prediction. Furthermore, the N and C termini of the cASIC1 open state structure as well as the C terminus of the desensitized state structure were extended by three additional residues in order to match the length of the closed state structure. Afterward, hASIC1a and lASIC models were built by threading their amino acid sequences through the structures of cASIC1 guided by pairwise amino acid sequence alignments created with ClustalW (Larkin et al., 2007). The following amino acids were changed in the lASIC model to reflect the changes that were made experimentally to the lASIC sequence in order to evoke large proton-mediated currents: C75H, Q79L, T87L, N347D, and M351D (Li et al., 2010c). hASIC1a and lASIC models were refined by minimization in Cartesian space with the RosettaMembrane energy function (Barth et al., 2007) while applying weak harmonic restraints to the positions of all backbone heavy atoms. C3 symmetry of the trimeric ASIC structure was enforced by means of symmetry definition files as described in DiMaio et al. (2011). Amino acid side chain positions were refined by a simulated annealing search algorithm, referred to as rotamer packing in Rosetta. Model quality was additionally checked by MolProbity (Davis et al., 2007) analysis, and the hASIC1a and lASIC models with best MolProbity and Rosetta scores were considered the final models.

Protein stability prediction for hASIC1a and lASIC mutants
Free energy changes of hASIC1a or lASIC structures owing to amino acid mutations at R64 or W66, respectively, were calculated with the Rosetta Flex ddG protocol (Barlow et al., 2018) and the RosettaMembrane all-atom energy function (Barth et al., 2007). RosettaMembrane employs an implicit membrane bilayer model, consisting of a hydrophobic core region of 18-Å thickness and transition regions of 6 Å on either side, and uses an implicit atomic solvation potential based on the model developed by (Lazaridis and Karplus, 2000, 2002). In short, the Flex ddG protocol models mutation-induced conformational and energetic changes by a series of "backrub" moves (15,000 steps in this study) of the protein backbone coupled to side chain repacking in an 8-Å shell around the mutation site, followed by minimization of all protein backbone and side chain degrees of freedom. This sampling method aims at improving the prediction for mutations with a large change in amino acid side chain volume. Afterward, structures were minimized in Cartesian space until convergence was reached and the change of the Rosetta score between subsequent iterations was <1.0 REU (Rosetta energy unit). To avoid large deviations from the input structure, Cα-atom pair distance restraints with a harmonic

Chen et al.
Arginine 64 sets stability of open and closed states in ASIC

Journal of General Physiology
https://doi.org/10.1085/jgp.202012802

2 of 14

penalty function were applied during minimization. A mutation was modeled in each of the three ASIC subunits simultaneously by enforcing C3 symmetry by means of Rosetta symmetry definition files. 50 separate Flex ddG trajectories were performed for each mutant and the WT, and the Rosetta energy change ($\Delta\Delta G$) was calculated as average score difference between the three top-scoring mutant and WT structures. Stability calculations were repeated at least 10 times for each hASIC1a and lASIC mutant, and the mean $\Delta\Delta G$ ($\pm$ SEM) was used for making stability predictions.

cDNA constructs and mutagenesis

Plasmid pcDNA3.1(–) containing hASIC1a-HA, lASIC-Flag, mouse ASIC2a-HA, and mouse ASIC3-HA served as templates for introducing point mutations using QuickChange according to manufacturer instructions. Chimeras were made using PCR and cDNAs of human ASIC1a and lamprey ASICs. Nucleotides of all constructs were verified by DNA sequencing.

Synthesis of complementary RNAs (cRNAs) and injection of *Xenopus laevis* oocytes

pcDNA3.1 plasmids containing ASIC cDNAs were linearized with HindIII followed by in vitro synthesis of RNA using mMESSAGEmMACHINE T7 according to the manufacturer's instructions. Concentration of RNA was adjusted to 300 ng/µl using Nanodrop. 5 ng cRNA solution were injected per oocyte followed by incubation at 18°C for 24–36 h before experiments. Oocytes were harvested from female *Xenopus* according to a protocol approved by the Institutional Animal Care and Use Committee of Tsinghua University (protocol no. 07749). The Association for Assessment and Accreditation of Laboratory Animal Care International has accredited the Tsinghua University amphibian animal facility. Harvested oocytes were treated with 20 mg/10 ml of collagenase for 30–40 min at room temperature. Cells were extensively washed, injected with cRNA, and incubated at 18°C.

Two-electrode voltage clamp

Whole-cell currents were measured using a two-electrode voltage clamp (Oocyte-Clamp OC-725C; Warner Instruments) with PowerLab 8/35 (ADInstruments) running LabChartPro software. Cells were placed in a fast exchange perfusion chamber with high flow delivered by gravity. Perfusion solutions had the following composition (in mM): 100 NaCl, 4 KCl, 1.5 CaCl$_2$, 10 HEPES, and 10 2-(N-morpholino) ethanesulfonic acid. pH was adjusted to desired values with N-methyl-D-glucamine. Pipette resistances were 0.5–1 MΩ when filled with 3 M KCl. Oocytes were voltage clamped at –60 mV. ASIC currents were activated by changing the external solution from a conditioning pH of 7.4, or any other indicated value, to a more acidic test pH for 30 s until currents completely desensitized or the sustained current reached a plateau. The external solution was returned to pH 7.4 or changed to the indicated preconditioning pH for 60 s. Apparent pH$_{50a}$ and pH$_{50}$ of SSD were calculated measuring the magnitude of currents elicited with pH solutions of various values from 7.4 to 5.0.

Patch clamp

Currents were recorded from excised patches in the outside-out configuration using a HEKA patch clamp EPC10 amplifier and PATCHMASTER acquisition software v2 × 90.2 (HEKA Electronic). Pipette solution contained (in mM) 100 KCl and 20 HEPES, pH 7.4. Bath solution contained (in mM) 100 NaCl, 4 KCl, 2 CaCl$_2$, and 20 HEPES/Mes adjusted to pH 7.4 or lower pH with NMDG. Membrane potential was held at –60 mV. Patches were perfused with a solution of pH 7.4 to establish the baseline current, followed by activation with low pH solutions using a fast-exchange perfusion system (SF-77B perfusion-step; Warner Instruments). Experiments were conducted at room temperature.

Data analysis

Concentration response curves were fit to the Hill function: $I = 1 / (1 + (10^{pH_{50a}} / 10^{pH})^n$, where pH$_{50a}$ is the pH at which the half-maximal activation/desensitization of the maximal current was achieved, and n is the Hill coefficient. The results are reported as mean $\pm$ SD. They represent the mean of 4–10 individual measurements in different oocytes and at least two different batches of oocytes. Statistically significant differences between groups were determined with Student's t test.

Online supplemental material

Fig. S1 is a cartoon representation of the putative desensitization mechanism mediated by the β11-β12 linker. Fig. S2 shows a comparison of Rosetta homology models of human and lamprey ASIC channels with experimental structures of cASICs. Fig. S3 shows cartoon representations of x-ray–determined structures of cASIC1a and Rosetta-predicted models of hASIC1a R64F. Fig. S4 shows a breakdown of computationally predicted protein stability changes for hASIC1a-R64 and lASIC-W66 mutants by Rosetta score term. Fig. S5 shows the effect of a reducing agent on the activity of S83C-Q358C CH1.

Results

Role of TM1 in the kinetics of proton gating of ASICs

ASICs from vertebrate species exhibit broad differences in apparent proton affinity and kinetics of desensitization despite overall sequence conservation; therefore, they provide a source to find out elements that are functionally significant. The evolutionary distant lamprey ASIC represents such an instance as it shares 70% amino acid identity with hASIC1a but exhibits significant functional differences. We previously showed that lASIC gains proton-mediated gating with two substitutions in the β1 strand, C75H and Q79L, but these channels display very high apparent proton affinity for activation and almost no desensitization from the open and preopen states (SSD; Li et al., 2010c). The lack of desensitization is intriguing because lASIC has the corresponding mammalian residues of the β11-β12 linker (L415 and N416), raising the question of what prevents the desensitization mechanism from working in lASIC. To address this question, we first replaced the whole ECD of lASIC with the one of hASIC1a (CH1). Fig. 1 A shows that CH1 displays large sustained currents similar to those of lASIC. Swapping of hASIC1a TM2 into lASIC (CH2) leaves channel properties intact, pointing to TM1 or the N and C termini as potential contributors to desensitization.

We focused on the outer half of TM1, where most of the differences between human and lamprey are present as

Chen et al.
Arginine 64 sets stability of open and closed states in ASIC

Journal of General Physiology   3 of 14
https://doi.org/10.1085/jgp.202012802
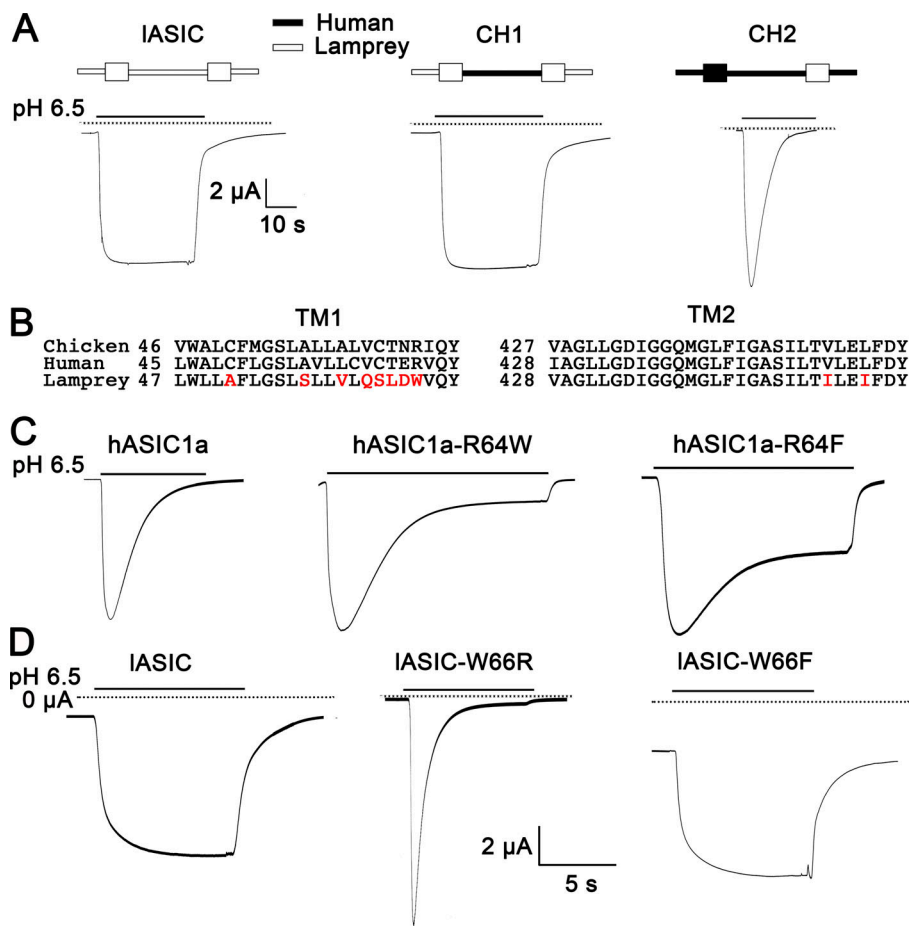
Figure 1. **Residue Trp-66 located close to the external side of TM1 in lASIC produces channels without desensitization.** **(A)** lASIC and functional chimeras (CH1 and CH2) made with sequences of hASIC1a are represented above the corresponding current traces activated by pH 6.5. The continuous line indicates duration of the stimulus and dashed line the zero-level current. The experiment was repeated three times with different batches of oocytes. 10 oocytes were examined for each chimera. **(B)** Alignment of TM1 and TM2 amino acid sequences of chicken, human, and lamprey ASIC channels. In red are residues present only in lamprey. **(C)** Replacement of Arg-64 by Trp or Phe in hASIC1 induces nondesensitizing currents. The experiment was repeated three times with different batches of oocytes. 10 oocytes were measured for each mutant. **(D)** Replacement of Trp-66 in lASIC (W64R) for the corresponding residue in hASIC1a produces complete desensitization, whereas replacement by another aromatic side chain (W66F) maintains desensitization and increases the level of constitutive current at pH 7.4. The experiment was repeated three times with different batches of oocytes. 10 oocytes were examined for each construct.

indicated in the alignment shown in Fig. 1 B. In red are residues unique to lamprey; therefore, they are the most likely to give rise to the observed functional differences. The analysis started with position R64 that was substituted first with W64 followed by other large hydrophobic residues. The following residues slowing desensitization were F>W>Y>L>M, with aromatics also inducing a component of sustained current (Table 1). Small amino acids (G, A, and C) and charged hydrophilic residues such as E and K exhibited complete desensitization (Table 1). Conversely, substitutions of W66 in lASIC by R, C, or A induced both forms of desensitization. Mutant R66[lASIC] exhibited fast (τ 1.4 s) and complete desensitization in contrast to mutant F66[lASIC], which was open 50% at pH 7.4 and did not display desensitization (Fig. 1 D). Replacement of each of the other red-labeled residues in hASIC1a for the lamprey counterpart produced functional channels with large currents but no sustained component. The pH$_{50}$ values and rates of desensitization are shown in Table 1.

These results indicate that arginine in both human R64[hASIC1a] and lamprey R66[lASIC] favors desensitization, whereas residues with large aromatic side chains produce channels with diminished desensitization.

Interactions of R64 and W66 in protein structure models of hASIC1a and lASIC

To help elucidate the structural role of TM1 residues R64 in hASIC1a and W66 in lASIC, structural models of both human and

lamprey ASICs in closed, open, and desensitized conformations were developed by homology modeling with Rosetta (Fig. 2, A and B). Crystal structures of cASIC (90% identical to hASIC1a and 72% identical to lASIC) in the closed (PDB accession no. 5WKV), open (PDB accession no. 4NTW), and desensitized (PDB accession no. 4NYK) states served as templates for homology modeling.

Within the transmembrane and ECDs, the homology models bear high similarity to their crystal structure templates (Fig. S2); the side chain RMSD in TM1 and TM2 is on average smaller than 2.0 Å. For modeling the open state, we used the MitTx-bound structure of cASIC1. This supports the conclusion that the pore domain structure of MitTx-bound cASIC1 likely represents the WT, proton-activated cASIC1 pore structure. In addition, removing MitTx from the cASIC1 template structure did not induce any large conformational changes in hASIC1a and lASIC models compared with the MitTx-bound cASIC1 starting structure, even when positional restraints on the protein backbone atoms were turned off, which indicates that the cASIC1 structure is not overly structurally constrained by MitTx.

In the homology models, R64 and W66 are located on the extracellular end of TM1, where they are ~12 Å away from the membrane center along the z direction (Fig. 2 A). Hence, their location is in the transition region between the hydrophobic membrane core and the soluble region.

In the hASIC1a structural model, R64 is surrounded by three aromatic residues (Y67, Y68, Y426) and several negatively

Chen et al.
Arginine 64 sets stability of open and closed states in ASIC

Journal of General Physiology 4 of 14
https://doi.org/10.1085/jgp.202012802

Table 1. **Properties of all ASIC mutants examined in this work**

Channel	pH_{50a}	n_a	pH_{50SSD}	n_{SSD}	I_s/I_p	τ_D (s)
hASIC1a						
WT	6.60 ± 0.18	4.5	7.1 ± 0.09	7.5	0.0	1.65 ± 0.15
R64G	6.23 ± 0.08	3.2	7.05 ± 0.07	4.2	0.0	1.0 ± 0.2
R64E	6.50 ± 0.05	4.8	7.1 ± 0.08	7.3	0.0	1.06 ± 0.05
R64K	6.60 ± 0.10	4.7	6.98 ± 0.01	7.8	0.17 ± 0.004	2.05 ± 0.2
R64C	6.61 ± 0.09	4.2	7.1 ± 0.05	7.3	0.0	2.5 ± 0.02
R64A	6.63 ± 0.02	3.6	7.14 ± 0.03	7.1	0.0	1.06 ± 0.1
R64M	6.84 ± 0.1	3.5	7.01 ± 0.07	8.0	0.0	6.8 ± 0.1
R64L	6.82 ± 0.06	6.5	7.0 ± 0.012	8.5	0.07 ± 0.002	6.6 ± 0.1
R64Y	7.06 ± 0.1	8.0	ND	ND	0.21 ± 0.02	6.5 ± 0.2
R64F	7.1 ± 0.1	7.4	ND	ND	0.77 ± 0.08	ND
R64W	7.09 ± 0.4	7.0	ND	ND	0.33 ± 0.09	7.8 ± 0.1
L58V	6.59 ± 0.1	4.8	7.1 ± 0.01	7.0	0.0	1.6 ± 0.15
V60Q	6.55 ± 0.12	4.5	7.1 ± 0.02	6.9	0.0	1.63 ± 0.02
C61S	6.5 ± 0.06	4.2	7.14 ± 0.05	7.2	0.0	1.59 ± 0.1
T62L	6.45 ± 0.08	4.9	7.17 ± 0.08	7.0	0.0	1.1 ± 0.09
E63D	6.58 ± 0.09	4.3	7.11 ± 0.07	6.8	0.0	1.6 ± 0.03
lASIC						
WT	7.21 ± 0.1	9.4	ND	ND	1.0	ND
W66R	6.8 ± 0.2	2.9	7.2 ± 0.005	11	0.0	1.4 ± 0.04
W66C	6.78 ± 0.1	2.6	7.1 ± 0.002	9.0	0.08 ± 0.01	1.85 ± 0.1
W66F	7.3 ± 0.2	9.4	ND	ND	1.0	ND
mASIC2						
WT	4.0 ± 0.2	2.0			0.22 ± 0.05	2.5 ± 0.05
R63F	6.0 ± 0.1	4.0			0.68 ± 0.08	
R63W	6.0 ± 0.3	4.0			0.69 ± 0.06	
mASIC3						
WT	6.0 ± 0.1	1.0			0.0	0.27 ± 0.07
R64F	7.0 ± 0.3	7.0			0.91 ± 0.06	

pH_{50a}, pH_{50} of activation; n_a, Hill coefficient of activation; pH_{50SSD}, pH_{50} of steady stead desensitization; n_{SSD}, n coefficient of SSD; I_s/I_p, ratio of sustained current/peak current both measured at pH_{50a}; t_D, 1/rate of desensitization from open state measured at pH_{50a} in seconds; N.D., not determined owing to absent or very weak desensitization. For channels exhibiting a fraction of sustained currents, t_D corresponds to the desensitizing component of the current fit to a single exponential. Each data point represents the mean of at least four measurements from independent cells ± SD.

charged or polar residues (E63, E427, D434, Q438; Fig. 2 C). In the closed and desensitized state, the side chain of R64 interacts with that of D434 in TM2a and is capped by the aromatic ring of Y426. As shown in Fig. S3 A, additional hydrogen bond interactions with E426 in TM2a of a neighboring subunit and with E63 on the same subunit also seem possible as observed in the cASIC1 crystal structures of the closed and desensitized states. In the open channel conformation, R64 extends further into the space created by the extracellular fenestration between two ASIC subunits that is formed by TM1 and TM2 translation in channel activation. In this state, R64 is stabilized by hydrogen bond interactions with E63 and D434 (Fig. 2 C).

In contrast to hASIC1a-R64, no hydrogen bonding is observed for W66 in the lASIC structural models. However, other potentially stabilizing interactions are made by W66 such as a face-to-edge stacking contact between its indole ring and the aromatic ring of Y467, and tight packing interactions with residues Y69, A429, L431, and I435 (Fig. 2 C). In the lASIC open state model, the TM1-TM2a inter-subunit interface is more expanded, which allows rearrangement of the side chains of Y426, D434, and Q438 around W66, and formation of additional hydrogen bonds between those residues. These hydrogen bond contacts probably contribute to the stability of the open state structure, but are absent in the closed and desensitized states.

Chen et al.
Arginine 64 sets stability of open and closed states in ASIC

Journal of General Physiology   5 of 14
https://doi.org/10.1085/jgp.202012802
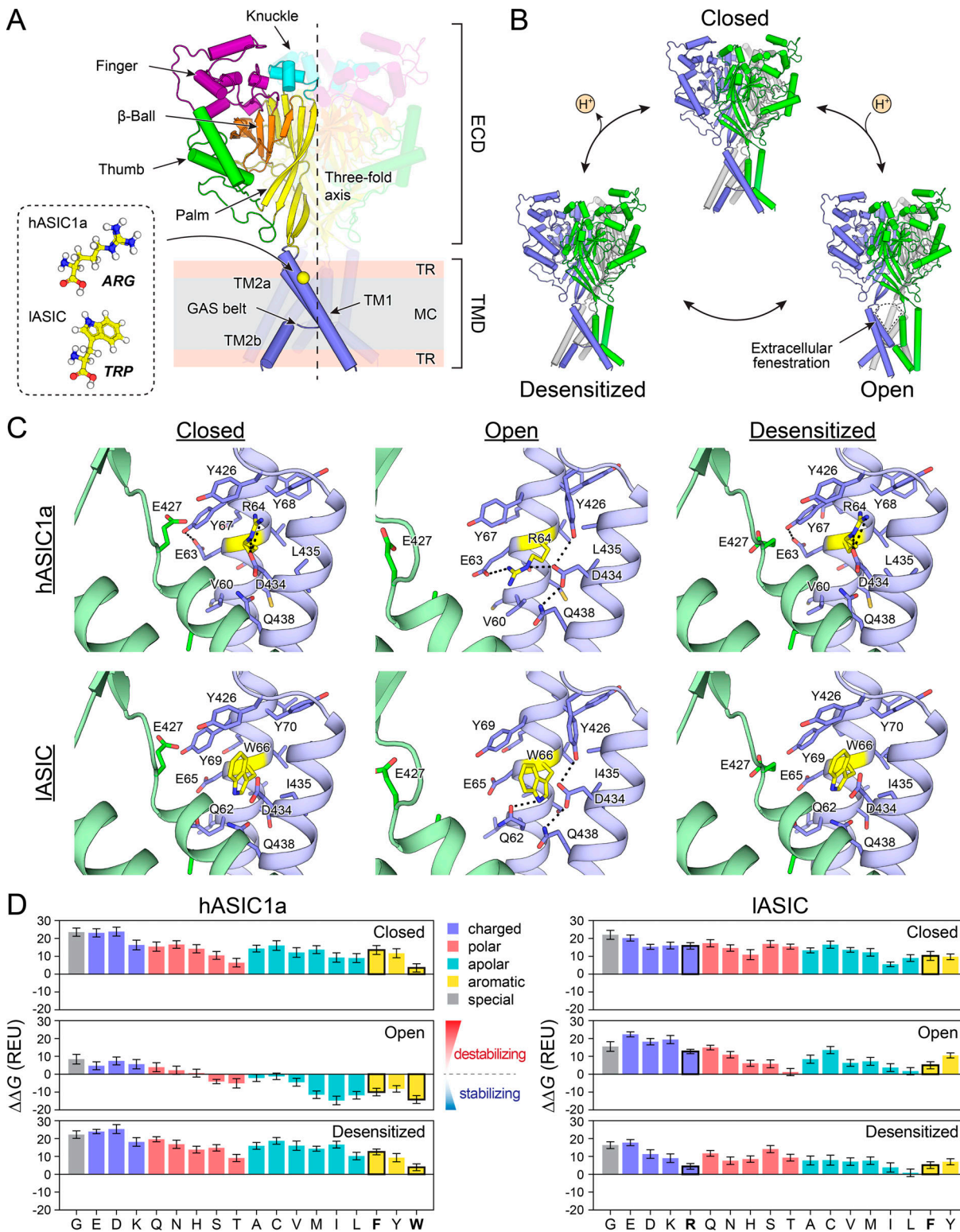
Figure 2. **Protein structure modeling and stability calculations suggest that large aliphatic and aromatic amino acids at positions 64/66 in hASIC1a/ lASIC favor the open channel conformation. (A)** Model of hASIC1a with each domain depicted with a different color. For clarity, only one subunit is shown and the other two subunits are transparent. The position of R64 (W66 in lASIC) on the outer segment of TM1 is shown as yellow sphere. The membrane is depicted schematically and divided into membrane core (MC), which corresponds to the region occupied by the fatty acid chains, and transition region (TR), which is the area occupied by the glycerol-phosphate and lipid head groups. TMD, transmembrane domain. **(B)** Homology models of hASIC1a in closed, open, and desensitized states and their interdependencies according to the proton-mediated gating cycle of ASICs. **(C)** Residues surrounding R64 in hASIC1a and W66 in lASIC in structural models of the closed, open, and desensitized states. For clarity, only two subunits, which make interactions with R64 or W66 in the depicted models, are shown and colored blue and green, respectively. Possible side chain hydrogen bonds are indicated as dashed lines. **(D)** Computationally

predicted stability changes (ΔΔG) for mutations of R64 in hASIC1a (left) or W66 in lASIC (right) to every other amino acid. A negative ΔΔG value indicates that protein stability relative to WT is increased by the mutation, whereas a positive value for ΔΔG indicates a destabilization. ΔΔG values for F/W64[hASIC1a] and R/F66[lASIC], for which currents are shown in Fig. 1, B and C, are indicated with a black frame. Values for proline were off-scale due to incompatible backbone geometries in the starting model and are not shown in the plots (hASIC1a closed: 60.2 ± 2.2 REU, open: 45.9 ± 2.2 REU, desensitized: 54.5 ± 1.9 REU; lASIC closed: 46.5 ± 2.4 REU, open: 56.2 ± 3.6 REU, desensitized: 47.7 ± 2.6 REU).

Structure-based energy calculations indicate that residue 64[hASIC1a]/66[lASIC] plays a role for the state-dependent stability of ASICs

To gain further mechanistic insight into the dual role of amino acid residues at positions 64 and 66 in hASIC1a and lASIC, respectively, we performed protein stability calculations with Rosetta. hASIC1a-R64 and lASIC-W66 were changed to every other amino acid, and the changes in the energy of the closed, open, and desensitized state structures were calculated (Fig. 2 D). Substitutions of R64 for amino acids with a charged or long polar side chain destabilize the hASIC1a structure of all three states. Amino acids with a small polar or apolar side chain destabilize the closed and desensitized state but have little effect on the stability of the open state, whereas amino acids with a large hydrophobic or aromatic side chain considerably increase the stability of the open state structure. Tryptophan at position 64 is predicted to lead to the strongest increase in the stability of the open state, but causes insignificant changes in stability of the closed and desensitized states. Mutation of R64 to F also increases the stability of the open state, but decreases the stability of the closed and desensitized states. These data are consistent with the observation that hASIC1a channels with either W or F at position 64 have higher open probability and higher apparent proton affinity compared with channels with R. Furthermore, differences in the stability of the desensitized state between R64F and R64W can explain why F slows desensitization of hASIC1a more than W.

Analysis of the forces implicated in state stability (Fig. S4) revealed two components that mostly contribute to the improved open state stability of hASIC1a with W versus R: (1) increased van der Waals attractive forces of F and W with surrounding residues, and (2) a favorable energy of transfer of F and W in the outer membrane region at the location of residue 64. Furthermore, the forces predicted to be most important for the stabilization of the closed and desensitized state by residue R64 are hydrogen bonds; the loss of these interactions when R is changed to amino acids that have no or lower capability of forming side chain hydrogen bonds leads to destabilization of the closed and desensitized states.

Substitutions at the corresponding position W66 in lASIC decrease the stability of all three states (Fig. 2 D); however, F and other hydrophobic amino acids (L, I) have a minimal effect on the stability of the open state structure and are similar to the WT. By contrast, substitution of W66 for R leads to a strong destabilization of the open state, but has a negligible effect on the stability of the desensitized state. These predictions match the experimental result, as R66[lASIC] produced rapid and complete desensitization whereas F66[lASIC] did not desensitize as WT lASIC and even had a larger fraction of channels open at neutral pH (50%), suggesting that destabilization of the closed state by F brings TM1 a step closer to the open conformation.

Similar to hASIC1a, analysis of the forces that contributed to the changes in the Rosetta energy (Fig. S4) showed that differences in the open state stability of lASIC with R versus W/F at position 66 are largely due to differences in the membrane environment energy, which is lower for W and F in the outer membrane transition region compared with R. Furthermore, side chain hydrogen bonding by R is important for the increased stability of the desensitized state of R66[lASIC].

Together, these results suggest that the opposing effects of R and aromatics at position 64/66 in hASIC1a/lASIC on the stability of the open versus the closed or desensitized state are determined by differences in nonbonded interactions and the energy associated with insertion into the membrane for these amino acids. Stabilization of the conformation of the open state and destabilization of the conformation of the desensitized state by aromatic amino acids can explain their dual role on the proton affinity of activation and the degree of desensitization.

Mutation Q278G reverts R66[lASIC] to a nondesensitizing channel

As indicated in Fig. 1, R66[lASIC] channels desensitize rapidly and completely; however, introduction of the additional mutation Q278G, a residue that is in the vicinity of the β11-β12 linker and alters its function (Wu et al., 2019), reverted the double mutant R66-G278[lASIC] to a nondesensitizing phenotype (Fig. 3 A). Desensitization from both the open and preopen conformations was fully restored (Fig. 3 B). The mutation Q278G added to lASIC did not change the currents: channels remained nondesensitizing. Conversely, the mutation F64 in hASIC1a reduced desensitization by half, and addition of Q276G further reduced desensitization at pH 6.0 (Fig. 3, C and D). These results show that W64[lASIC] and F64[hASIC1a] both have a functional β11-β12 linker, but is not fully activated while the pore remains open.

F64[hASIC1a] exhibits long openings and a subconductance state

To gain more insight in the mechanism underlying decreased desensitization and to experimentally test the predictions from Rosetta calculations, we examined single channel activity of F64[hASIC1a] in excised membrane patches activated with low proton concentrations, pH in the range of 7.3 to 7.1. Fig. 4 A shows a typical current trace of a patch expressing many channels (~400 channels) exposed to pH 7.1 for 1 min. About half the magnitude of the peak current remains as a sustained component through the duration of the stimulus. We also examined numerous patches containing one or two channels (Fig. 4 B). A main finding was increased duration of opening events compared with WT hASIC1a (Fig. 4 F). Most of the recorded openings lasted >1 s and some up to 35 s. For comparison, Fig. 4 E shows examples of WT hASIC1a patches containing numerous channels or single channel activity. Notice the time scale in Fig. 4 F is 100-fold smaller than for the mutant. Traces

Chen et al.
Arginine 64 sets stability of open and closed states in ASIC

Journal of General Physiology   7 of 14
https://doi.org/10.1085/jgp.202012802
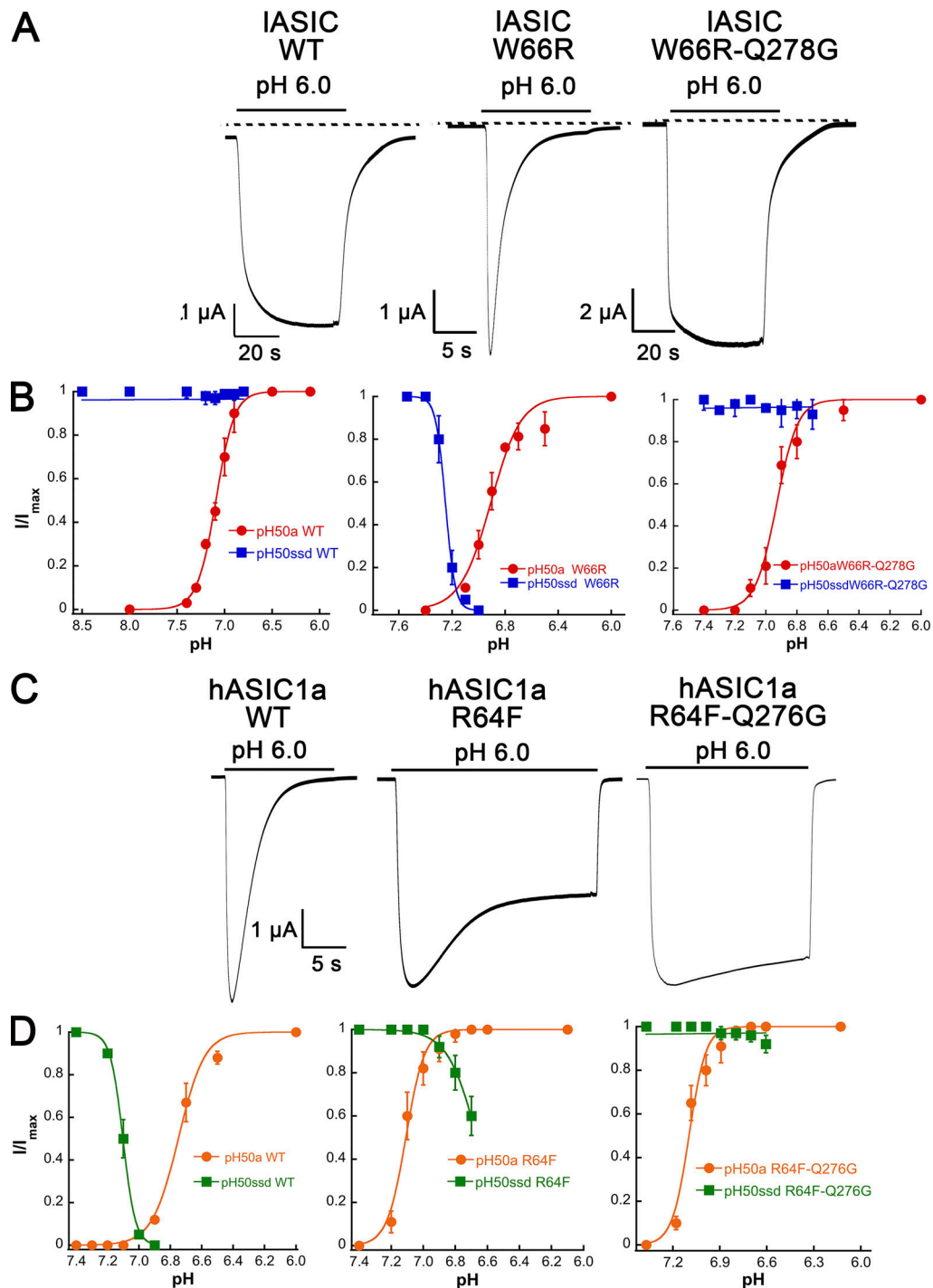
Figure 3. **R64[hASIC1a] and R66[lASIC] enable channel desensitization by the β11-β12 linker mechanism. (A)** Representative lASIC current traces exhibiting sustained currents in the presence of pH 6.0. The substitution R66[lASIC] in the outer segment of TM1 produces rapid and complete desensitization upon exposure to pH 6.0, which is reverted back to nondesensitizing when the β11-β12 linker mechanism is disabled by the mutation Q278G. **(B)** Increasing proton concentration response curves of activation (red curve) and SSD (blue curve) currents. Lines are the fit to the Hill function. Each data point represents four to seven independent measurements. **(C)** Typical proton-induced current of hASIC1a WT desensitizes completely. Channels with the substitution R64F exhibit slow and incomplete desensitization. Impairing function of the β11-β12 linker by the mutation Q276G eliminates desensitization in hAQSIC1a-R64F-Q276G. **(D)** Concentration response curves of channel activation (orange curve) and SSD (green curve) shown in C fit to the Hill function. Each data point represents four to five independent measurements.

Chen et al.
Arginine 64 sets stability of open and closed states in ASIC

Journal of General Physiology 8 of 14
https://doi.org/10.1085/jgp.202012802
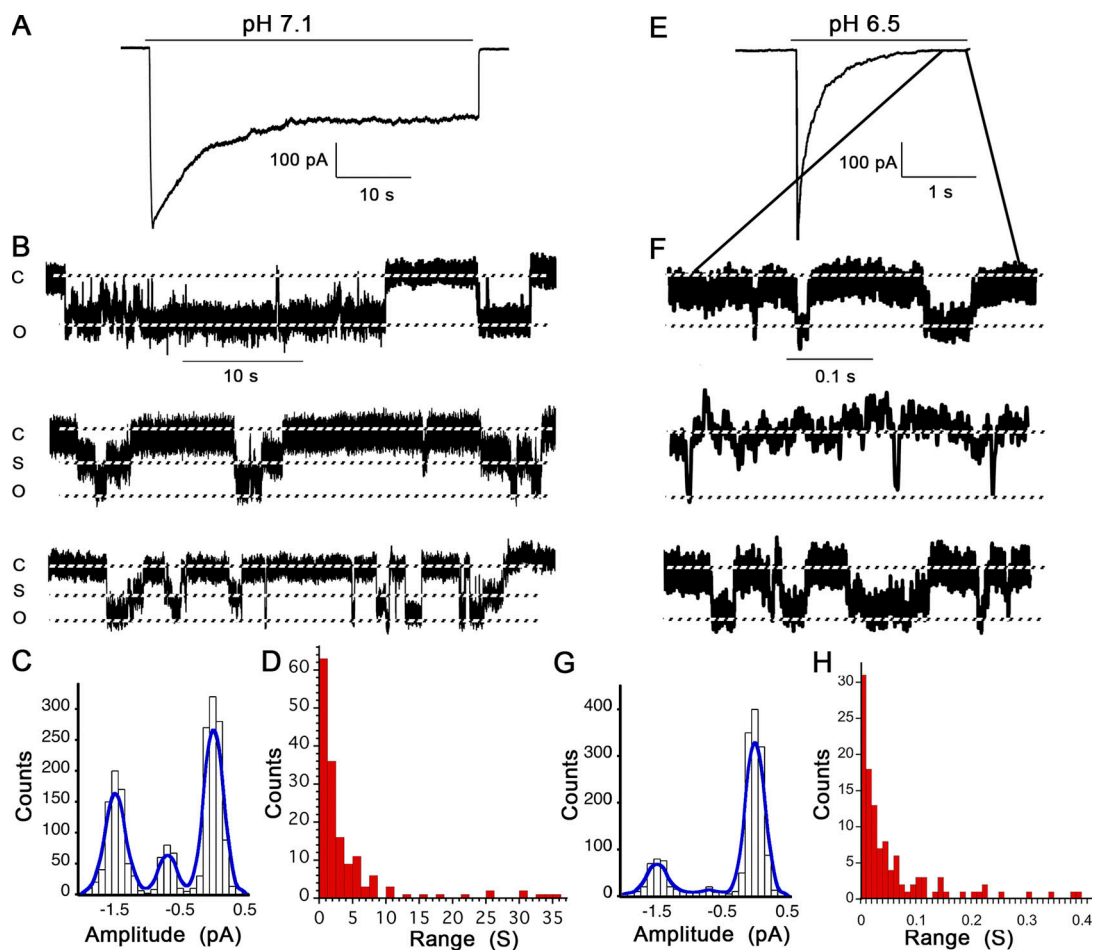
Figure 4.   **F64^hASIC1a exhibits long opening events and a subconductance state. (A)** Representative example of an excised outside-out membrane patch containing a large number of channels activated by external pH 7.1 for 1 min. **(B)** Representative example of excised outside-out membrane patches containing a single channel activated by pH 7.2. Dashed lines indicate three current levels: closed (C), subconductance (S), and fully open (O). The subconductance state appears when channels transition to the open and to the closed states. Holding potential, −60 mV. External solution 100 mM Na$^+$; pipette solution 100 mM K$^+$. The shown trace represents 1 out of 15 patches, all showing the subconductance state. **(C)** All-points histogram of a continuous recording of activity of a single channel exhibits three conductance states of magnitude: 0, 0.7, and 1.5 pA. The line is the Gaussian fit to the data. **(D)** Histogram of duration of opening events in seconds. **(E)** Representative example of multichannel hASIC1a patch activated with pH 6.5. **(F)** Representative examples of unitary currents. **(G)** All-points histogram of a continuous recording of activity of a single channel exhibits two conductance states of magnitude: 0 and 1.5 pA. **(H)** Histogram of duration of opening events of WT hASIC1a.

showing unitary currents were obtained from multi-channel patches when the current approaches the zero level as indicated in Fig. 4 E. Analysis of the distribution of opening event's duration, histograms of Fig. 4, D–H, shows a 100-fold longer duration in F64^hASIC1a than in WT channels (3,000 ms versus 30 ms). These results indicate that F64^hASIC1a exhibits long open events and confirm the prediction that aromatic residues in position 64 stabilize the open conformation (Fig. 2 D).

The second finding was detection of a frequent subconductance state about half the amplitude of the fully open channel (0.7 pA) in patches activated by pH 7.3 and 7.1, the range of pH where individual channel activity was most frequently detected. Fig. 4 B shows that channels either enter directly the full open state or first enter the subconductance followed by a second transition to fully open while some openings visit only the subconductance state. Similarly, transitions from the open to closed state were detected directly to the fully shut state or in two steps: first subconductance

followed by completely shut. Only two conducting states were detected of amplitude 1.5 and 0.7 pA determined by all-points histograms of traces expressing single channels (Fig. 4 C). We cannot rule out the presence of additional subconductances of smaller amplitudes that were not resolved given the noise level of our current records. Various mechanisms give rise to ion channel subconductances; however, under the experimental conditions of low proton concentrations, the most parsimonious interpretation of the presence of a novel subconductance in F64^hASIC1a is that they represent currents generated by partially open channels (Chapman and VanDongen, 2005; Jin et al., 2003), i.e., channel openings with only one or two proton-bound subunits in the trimer.

Residue 64^hASIC1a/66^lASIC alters the apparent proton-affinity of ASIC1, ASIC2, and ASIC3s

The amino acid in position 64 of TM1 also changes the apparent pH$_{50a}$ of hASIC1a, namely, hydrophobic large side chains
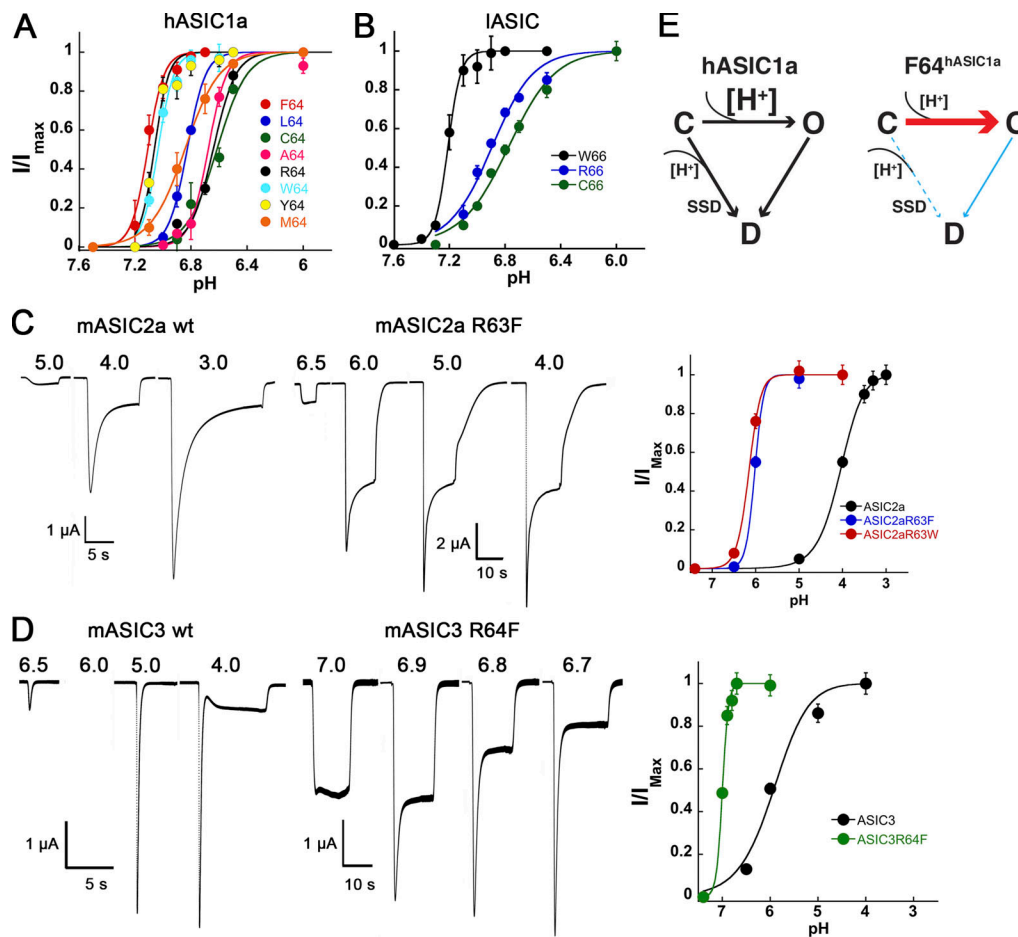
Figure 5. **Large hydrophobic residues at positions 64/66 in hASIC1a/lASIC increase the apparent pH$_{50a}$ of ASICs. (A)** Proton concentration-response curves of hASIC1a with various amino acid substitutions in position R64. Each data point represents the mean of four or five independent measurements ± SD. Mutants were measured in different experiments, but each one always had as control a group of WT oocytes to ensure the pH of solutions for activation were correctly calibrated; thus, the number of cells of the WT curve is 38. Curves are fit to the Hill equation. Values of pH$_{50a}$ and n (Hill coefficient) are presented in Table 1. **(B)** Proton concentration-response curves of lASIC1 with Arg or Cys substituting Trp-66. Lines in A and B are the fit of the data to the Hill equation. Each data point is the mean of four to six independent measurements. Error bars represent the SD. **(C)** Representative examples of currents activated by increasing concentration of protons of mASIC2a wt and the mutant mASIC2a-R63F and the corresponding concentration-response curves of activation. Each data point represents the average of at least five independent cells; error bars represent the SD. Lines are the fit to the Hill equation. **(D)** Representative examples of currents activated by increasing concentration of protons of mASIC3 wt and mutant mASIC3-R64F and the corresponding concentration-response curves of activation. Each data point represents the average of at least three independent cells; error bars represent the SD. Lines are fit to the Hill equation. **(E)** Simple kinetic schemes comparing WT and F64^{hASIC1a} response to high and low proton concentrations indicated by large- and small-type size [H$^+$]. Only three states are shown: C, closed; O, open; D, desensitized. The thick red arrow indicates the favored pathway, i.e., opening rather than SSD. The thin blue arrows indicate transitions that are slowed or markedly unfavored (broken line) by F64. wt, wild type.

increase the apparent sensitivity to protons (Fig. 5 A). F64^{hASIC1a} displays a pH$_{50a}$ of 7.1 compared with 6.6 of WT hASIC1a. Substitutions of the equivalent residue W66 in lASIC also change the pH$_{50a}$, but the shift is toward a lower pH range: W66^{lASIC} pH$_{50a}$ is 7.2, whereas that of R66^{lASIC} is 6.8 (Fig. 5 B).

We also sought to examine whether substitution of arginine for aromatic amino acids in ASIC2 and ASIC3 reproduces the functional effects observed in ASIC1a. For these experiments, mouse channels were used because their properties have been extensively characterized in contrast to the corresponding human isoforms, and the sequences are highly conserved with human (ASIC2a, 99.7% identity; ASIC3, 83%; Joeres et al., 2016; Zhang and Canessa, 2002). We introduced the mutations R63F/W^{mASIC2a} and R64F^{mASIC3}; functional analysis of R63F/W^{mASIC2a}

shows that the mutant generates large currents that display a much larger fraction of sustained current than WT (Fig. 5 C). The ratio of sustained/peak currents at pH$_{50a}$ is 0.22 ± 0.05 in WT mASIC2 and 0.68 ± 0.08 in the mutants, consistent with attenuation of desensitization. In addition, mutants exhibit a marked increase in proton affinity represented by a shift in pH$_{50a}$ from 4.0 to 6.0. Similar effects are observed in R64F^{mASIC3}: these channels are functional, exhibit large sustained currents, and are more sensitive to protons with a shift in pH$_{50a}$ from 6.0 to 7.0 and steeper activation curve (Hill coefficient mutant, $n = 7$; versus WT, $n = 1$; Fig. 5 D and Table 1). Together these results indicate that an aromatic residue in the corresponding position 64 in TM1 of ASICs, from chordates to the three mammalian isoforms, facilitates channel opening leading to high apparent

proton affinity of activation (red thick arrow, Fig. 5 E), prevents SSD (thin-dashed blue arrow, Fig. 5 E), and stabilizes the open conformation leading to reduced desensitization (thin blue arrow, Fig. 5 E).

Is the thumb involved in lASIC activation?

The previous sections show that lASIC1, CH1, and F64[hASIC1a] all gate with much lower concentrations of protons than hASIC1a despite sharing very similar or identical ECDs with hASIC1a, and therefore, the same proton sensor(s). To examine whether low proton-mediated gating of these channels entails similar conformational changes to ASICs that gate with high concentrations of protons, we examined specifically displacement of the thumb domain. To that end, the thumb domain was immobilized with a disulfide bond in lASIC and CH1. Two cysteines were introduced in the corresponding positions of cASIC that were previously used by Yoder et al. (2018) for this purpose: P85C-Q358C[lASIC] and S83C-Q358C[CH1]. lASIC and CH1 bearing two cysteines in the indicated positions both expressed very small currents, on average 0.69 ± 0.56 and 0.91 ± 0.53 µA/cell. After the same cells were treated with the sulfhydryl reducing agent Tris carboxy-ethyl-phosphate (TCEP) for ~1 h, currents increased to 5.2 ± 2.5 and 6.1 ± 1.5 µA/cell. Short treatment of <5 min applied in the perfusion chamber of the TEVC setup did not immediately increase current. Fig. 6, A and B, and Fig. S5 show typical examples of cells expressing P85C-D358C[lASIC] and S83C-Q358C[CH1] before and after treatment with TCEP and the average response of 10 independent cells. Oocytes expressing WT lASIC1 received the same treatment and served as the control (Fig. 6, C and D). The increase in current magnitude after TCEP treatment observed only in the double cysteine mutants is consistent with the interpretation that low proton concentrations induce conformational changes in both lASIC and CH1 that include movement of the thumb as in cASIC.

Discussion

The key finding of this work is that residue R64 in the outer segment of TM1 impacts the value of the apparent pH_{50a}, activation and desensitization of ASIC channels. Below we outline the mechanisms underlying the observations and how they enhance understanding of the activation and desensitization processes of ASICs.

High apparent pH_{50a} and enhanced proton-mediated gating

Aromatic side chains W/F in the outer segment of TM1 shift the conformational equilibrium toward the conductive state, facilitating pore opening. Other residues such as L and M also decrease the energy barrier of activation, although to a lower degree (Fig. 5 A). Two findings underlie the above effects: an increase in the value of the apparent pH_{50}, and channels conducting with one/two proton occupied subunits revealed by the presence of a subconductance in F64[hASIC1a]. Typically, single channel recordings show two states: open and shut. Considering that ASIC1a has three identical pore-forming subunits, the classical interpretation is that the conduction pathway is not formed unless all three subunits are in the active position,
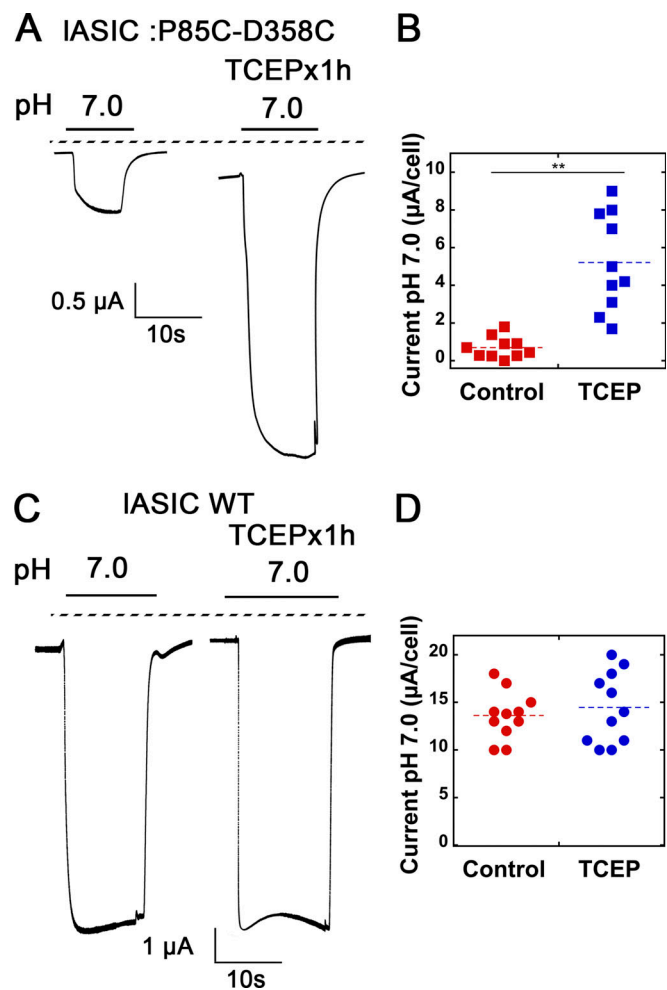
Figure 6. **Opening of lASIC, CH1, and F64[hASIC1a] with low proton concentrations is associated with movement of the α5-helix. (A)** Representative currents of lASIC P85C-D358C double mutant stimulated by pH 7.0 before and after treatment with 5 mM of the disulfide-reducing agent TCEP for 1 h. Dashed line is zero current level. **(B)** Maximal currents elicited by pH 7.0 in 10 independent cells expressing lASIC P85C-D358C before and after treatment with TCEP. Horizontal dashed lines indicate the mean current value. Asterisks represent significant statistical difference, **, P = 0.0003. **(C)** Representative currents of lASIC before and after treatment with TCEP for 1 h. **(D)** Values of maximal current elicited by pH 7.0 before and after TCEP treatment of 10 independent cells expressing lASIC.

i.e., all three are protonated. However, we detected frequent and long-lived intermediate current levels in channels exposed to pH 7.3–7.2 that are consistent with the ion pathway formed by only one or two proton-bound subunits instead of the three proton-bound subunits required for full conduction. Partial pore opening by activation of only a few of all the pore-forming subunits has been previously documented in voltage-activated (Chapman and VanDongen, 2005) and ligand-gated channels (Jin et al., 2003). Aromatics in the equivalent position in channels from early vertebrates (lASIC) to mammalian ASIC1a, ASIC2a, and ASIC3 also increase the efficacy of proton gating, underscoring the importance of R64 in setting the apparent pH_{50a}.

The previous observation also shows that the values measured as apparent proton affinities of activation are much lower

Chen et al.
Arginine 64 sets stability of open and closed states in ASIC

Journal of General Physiology 11 of 14
https://doi.org/10.1085/jgp.202012802

than the acid dissociation constant values of the proton binding site(s) involved in gating. According to our findings, the affinity of the site(s) has to be in the pH range 7.2–7.1 if not higher (such as in lASIC). Fig. 5 shows how various substitutions of R64 generate a range of apparent pH_{50a} in hASIC1a even though the proton binding site(s) remains the same. Thus, lowering the energy barrier of activation by replacing a single residue seems to be an effective strategy for tuning the apparent pH_{50a} and simpler than changing the affinity of one or more proton sensor(s). We noticed that R64 is highly conserved in ASICs from cartilaginous fishes to other branches of vertebrates with the exception of ASIC4, which has either no or small currents in zebrafish (Chen et al., 2007), suggesting that evolution selects for low proton sensitivity of ASICs. In contrast, other channels from the ENaC/Degenerin family with proton-independent gating and weak or no desensitization favor hydrophobic large/small side chains. In those channels, the position R64 is occupied by residues indicated here in parentheses: BLINAC(L), ENaC(F/L), FaNaC(L), and in many Degenerins(V/L). However, in ASICs, medium/large hydrophobic side chains not only shift the pH_{50} to more alkaline values but also weaken desensitization, representing a potential drawback to the use of such a strategy.

Desensitization

The observation that $F64^{hASIC1a}/W66^{lASIC}$ gate with proton concentrations in a range that induces SSD in most ASICs (pH ~7.2–7.1) rather than the usual low pH (~6.6–6.0), raises the question: Are activation and SSD two different processes driven by different sensors? Our results shed light on these questions by providing evidence that the two processes and the sensor that drives them may be the same.

Desensitization from the open state

Here, we show that stabilization of the open conformation by $F64^{hASIC1a}$ and $W66^{lASIC}$ markedly diminishes desensitization from the open state in the continuous presence of protons. This effect is completely reversible if the stabilizing residues in positions 66/64 are replaced by R, indicating that the β11-β12 linker desensitization mechanism and any other structures inducing desensitization are functional. It is also known that substitutions of a conserved glycine in TM2 that forms the gate of ENaC/Degenerin channels (G433DIGG; Gonzales et al., 2009) by residues with large side chains interfere with closure of the pore and eliminate ASIC2a/ASIC2b channel desensitization (Waldmann et al., 1996; Ugawa et al., 2001). Additionally, MitTx not only is a potent agonist that opens ASICs but also stabilizes the open conformation and prevents desensitization, as illustrated by the crystal structure of cASIC in complex with MitTx (PDB accession no. 4NTW). It shows the pore in open conformation and the β11-β12 linker in the nondesensitized conformation. From these lines of evidence, we reason that the pore must close to enable desensitization and β11-β12 linker isomerization.

Our results, however, have not elucidated the precise mechanism of how aromatic residues in the outer segment of TM1 stabilize the open channel conformation. The side chain of residue R64 faces the interior of the pore in all cASIC structures,

and the models of l ASIC and hASIC1a in closed, open, and desensitized states also predict W66/F64 side chains facing the interior of the pore. So we think it is unlikely that W66/F64 is in contact with the lipid bilayer. Instead, energy calculations and experimental evidence are consistent with W66/F64 having interactions with neighboring residues that alter the stability of the various conformational states.

Desensitization from the closed state: SSD

The question of whether the mechanism of SSD differs from that of desensitization from the open state, however, remains. Our results provide clues that both are probably similar with an important distinction. The evidence stems from the finding that very low concentration of protons enable opening of $F/W64^{hASIC1a}$. Since these channels are identical to WT hASIC1a (except for a single substitution in TM1), it is reasonable to expect that pH in the range 7.2–7.1 induces the same open conformation in hASIC1 as in $F/W64^{hASIC1a}$. The difference is that in WT channels, the ECD conformational change fails to open the pore because R64 presents a higher energy barrier of activation than F64. Since the pore remains closed, the lower palm contracts and locks the β11-β12 linker in the desensitized conformation. The end result is SSD rather than opening. Mechanistically, the most significant contribution of $F64^{hASIC1a}$ is that it makes visible a gating transition that is electrically silent in WT channels, i.e., low proton concentrations open $F64^{hASIC1a}$, whereas they induce SSD—an electrically silent transition—in WT hASIC1a.

As the predicted expansion and contraction of the lower palm elicited by low proton concentrations in hASIC1a subunits are electrically silent and too transient to be captured in atomic structures, additional evidence could be obtained from conformational dynamic approaches with high time resolution such as molecular dynamic simulations and patch fluorometry. Currently, there is some evidence from conformational dynamics studies using voltage-clamp fluorometry (Vullo et al., 2017), molecular dynamics simulations (Roy et al., 2013), and luminescence resonance energy transfer (Ramaswamy et al., 2013) supporting conformational changes in various parts of the ECD from the closed to open states such as shortening of the distance between the thumb and finger (Ramaswamy et al., 2013) and from the open to desensitized states such as contraction of the lower palm domain (Vullo et al., 2017). Less information is available of conformational changes from the closed to the SSD state. However, comparison of cryo-EM structures of cASIC in SSD (pH 7.0) and crystal structure in the desensitized state at pH 6.0 shows remarkable resemblance of the two forms of desensitization: collapse of the acidic pocket by the thumb domain, small rotation of the whole ECD, slightly contracted lower palm, and closed pore, consistent with the notion that channels end up in the same desensitized conformation whether exposed to low or high concentrations of protons.

To summarize, we have discussed here the main results, their functional significance, and, together with previous functional and structural data, put forward a plausible and parsimonious mechanism of ASIC desensitization and gating by low concentrations of protons.

Acknowledgments

References

Baconguis, I., C.J. Bohlen, A. Goehring, D. Julius, and E. Gouaux. 2014. X-ray structure of acid-sensing ion channel 1-snake toxin complex reveals open state of a Na⁺-selective channel. *Cell.* 156:717–729. https://doi.org/10.1016/j.cell.2014.01.011

Barlow, K.A., S. Ó Conchúir, S. Thompson, P. Suresh, J.E. Lucas, M. Heinonen, and T. Kortemme. 2018. Flex ddG: Rosetta ensemble-based estimation of changes in protein-protein binding affinity upon mutation. *J. Phys. Chem. B.* 122:5389–5399. https://doi.org/10.1021/acs.jpcb.7b11367

Barth, P., J. Schonbrun, and D. Baker. 2007. Toward high-resolution prediction and design of transmembrane helical protein structures. *Proc. Natl. Acad. Sci. USA.* 104:15682–15687. https://doi.org/10.1073/pnas.0702515104

Bohlen, C.J., A.T. Chesler, R. Sharif-Naeini, K.F. Medzihradszky, S. Zhou, D. King, E.E. Sánchez, A.L. Burlingame, A.I. Basbaum, and D. Julius. 2011. A heteromeric Texas coral snake toxin targets acid-sensing ion channels to produce pain. *Nature.* 479:410–414. https://doi.org/10.1038/nature10607

Chapman, M.L., and A.M.J. VanDongen. 2005. K channel subconductance levels result from heteromeric pore conformations. *J. Gen. Physiol.* 126:87–103. https://doi.org/10.1085/jgp.200509253

Chassagnon, I.R., C.A. McCarthy, Y.K. Chin, S.S. Pineda, A. Keramidas, M. Mobli, V. Pham, T.M. De Silva, J.W. Lynch, R.E. Widdop, et al. 2017. Potent neuroprotection after stroke afforded by a double-knot spider-venom peptide that inhibits acid-sensing ion channel 1a. *Proc. Natl. Acad. Sci. USA.* 114:3750–3755. https://doi.org/10.1073/pnas.1614728114

Chen, X., G. Polleichtner, I. Kadurin, and S. Gründer. 2007. Zebrafish acid-sensing ion channel (ASIC) 4, characterization of homo- and heteromeric channels, and identification of regions important for activation by H⁺ *J. Biol. Chem.* 282:30406–30413. https://doi.org/10.1074/jbc.M702229200

Davis, I.W., A. Leaver-Fay, V.B. Chen, J.N. Block, G.J. Kapral, X. Wang, L.W. Murray, W.B. Arendall III, J. Snoeyink, J.S. Richardson, and D.C. Richardson. 2007. MolProbity: all-atom contacts and structure validation for proteins and nucleic acids. *Nucleic Acids Res.* 35(Web Server):W375–W383. https://doi.org/10.1093/nar/gkm216

Deval, E., and E. Lingueglia. 2015. Acid-Sensing Ion Channels and nociception in the peripheral and central nervous systems. *Neuropharmacology.* 94:49–57. https://doi.org/10.1016/j.neuropharm.2015.02.009

DiMaio, F., A. Leaver-Fay, P. Bradley, D. Baker, and I. André. 2011. Modeling symmetric macromolecular structures in Rosetta3. *PLoS One.* 6:e20450. https://doi.org/10.1371/journal.pone.0020450

Du, J., M.P. Price, R.J. Taugher, D. Grigsby, J.J. Ash, A.C. Stark, M.Z. Hossain Saad, K. Singh, J. Mandal, J.A. Wemmie, and M.J. Welsh. 2017. Transient acidosis while retrieving a fear-related memory enhances its lability. *eLife.* 6:e22564. https://doi.org/10.7554/eLife.22564

Gonzales, E.B., T. Kawate, and E. Gouaux. 2009. Pore architecture and ion sites in acid-sensing ion channels and P2X receptors. *Nature.* 460:599–604. https://doi.org/10.1038/nature08218

González-Inchauspe, C., F.J. Urbano, M.N. Di Guilmi, and O.D. Uchitel. 2017. Acid-sensing ion channels activated by evoked released protons modulate synaptic transmission at the mouse Calyx of held synapse. *J. Neurosci.* 37:2589–2599. https://doi.org/10.1523/JNEUROSCI.2566-16.2017

Huang, P.-S., Y.-E.A. Ban, F. Richter, I. Andre, R. Vernon, W.R. Schief, and D. Baker. 2011. RosettaRemodel: a generalized framework for flexible backbone protein design. *PLoS One.* 6:e24109. https://doi.org/10.1371/journal.pone.0024109

Jasti, J., H. Furukawa, E.B. Gonzales, and E. Gouaux. 2007. Structure of acid-sensing ion channel 1 at 1.9 A resolution and low pH. *Nature.* 449:316–323. https://doi.org/10.1038/nature06163

Jin, R., T.G. Banke, M.L. Mayer, S.F. Traynelis, and E. Gouaux. 2003. Structural basis for partial agonist action at ionotropic glutamate receptors. *Nat. Neurosci.* 6:803–810. https://doi.org/10.1038/nn1091

Joeres, N., K. Augustinowski, A. Neuhof, M. Assmann, and S. Gründer. 2016. Functional and pharmacological characterization of two different ASIC1a/2a heteromers reveals their sensitivity to the spider toxin PcTx1. *Sci. Rep.* 6:27647. https://doi.org/10.1038/srep27647

Jones, D.T. 1999. Protein secondary structure prediction based on position-specific scoring matrices. *J. Mol. Biol.* 292:195–202. https://doi.org/10.1006/jmbi.1999.3091

Krauson, A.J., and M.D. Carattino. 2016. The thumb domain mediates acid-sensing ion channel desensitization. *J. Biol. Chem.* 291:11407–11419. https://doi.org/10.1074/jbc.M115.702316

Kreple, C.J., Y. Lu, R.J. Taugher, A.L. Schwager-Gutman, J. Du, M. Stump, Y. Wang, A. Ghobbeh, R. Fan, C.V. Cosme, et al. 2014. Acid-sensing ion channels contribute to synaptic transmission and inhibit cocaine-evoked plasticity. *Nat. Neurosci.* 17:1083–1091. https://doi.org/10.1038/nn.3750

Larkin, M.A., G. Blackshields, N.P. Brown, R. Chenna, P.A. McGettigan, H. McWilliam, F. Valentin, I.M. Wallace, A. Wilm, R. Lopez, et al. 2007. Clustal W and Clustal X version 2.0. *Bioinformatics.* 23:2947–2948. https://doi.org/10.1093/bioinformatics/btm404

Lazaridis, T., and M. Karplus. 2000. Effective energy functions for protein structure prediction. *Curr Opin Struct Biol.* 10:139–145. https://doi.org/10.1016/s0959-440x(00)00063-4

Lazaridis, T., and M. Karplus. 2002. Thermodynamics of protein folding: a microscopic view. *Biophys Chem.* 100:367–395. https://doi.org/10.1016/S0301-4622(02)00293-4

Leman, J.K., B.D. Weitzner, S.M. Lewis, J. Adolf-Bryfogle, N. Alam, R.F. Alford, M. Aprahamian, D. Baker, K.A. Barlow, P. Barth, et al. 2020. Macromolecular modeling and design in Rosetta: recent methods and frameworks. *Nat. Methods.* 17:665–680. https://doi.org/10.1038/s41592-020-0848-2

Li, T., Y. Yang, and C.M. Canessa. 2009. Interaction of the aromatics Tyr-72/Trp-288 in the interface of the extracellular and transmembrane domains is essential for proton gating of acid-sensing ion channels. *J. Biol. Chem.* 284:4689–4694. https://doi.org/10.1074/jbc.M805302200

Li, T., Y. Yang, and C.M. Canessa. 2010a. Leu85 in the β1-β2 linker of ASIC1 slows activation and decreases the apparent proton affinity by stabilizing a closed conformation. *J. Biol. Chem.* 285:22706–22712. https://doi.org/10.1074/jbc.M110.134114

Li, T., Y. Yang, and C.M. Canessa. 2010b. Asn415 in the β11-β12 linker decreases proton-dependent desensitization of ASIC1. *J. Biol. Chem.* 285:31285–31291. https://doi.org/10.1074/jbc.M110.160382

Li, T., Y. Yang, and C.M. Canessa. 2010c. Two residues in the extracellular domain convert a nonfunctional ASIC1 into a proton-activated channel. *Am. J. Physiol. Cell Physiol.* 299:C66–C73. https://doi.org/10.1152/ajpcell.00100.2010

Paukert, M., X. Chen, G. Polleichtner, H. Schindelin, and S. Gründer. 2008. Candidate amino acids involved in H+ gating of acid-sensing ion channel 1a. *J. Biol. Chem.* 283:572–581. https://doi.org/10.1074/jbc.M706811200

Ramaswamy, S.S., D.M. MacLean, A.A. Gorfe, and V. Jayaraman. 2013. Proton-mediated conformational changes in an acid-sensing ion channel. *J. Biol. Chem.* 288:35896–35903. https://doi.org/10.1074/jbc.M113.478982

Rook, M.L., M. Musgaard, and D.M. MacLean. 2020a. Coupling structure with function in acid-sensing ion channels: challenges in pursuit of proton sensors. *J. Physiol.* https://doi.org/10.1113/JP278707

Rook, M.L., A. Williamson, J.D. Lueck, M. Musgaard, and D.M. Maclean. 2020b. β11-12 linker isomerization governs acid-sensing ion channel

desensitization and recovery. *eLife.* 9:e51111. https://doi.org/10.7554/eLife.51111

Roy, S., C. Boiteux, O. Alijevic, C. Liang, S. Bernèche, and S. Kellenberger. 2013. Molecular determinants of desensitization in an ENaC/degenerin channel. *FASEB J.* 27:5034–5045. https://doi.org/10.1096/fj.13-230680

Sherwood, T.W., and C.C. Askwith. 2009. Dynorphin opioid peptides enhance acid-sensing ion channel 1a activity and acidosis-induced neuronal death. *J. Neurosci.* 29:14371–14380. https://doi.org/10.1523/JNEUROSCI.2186-09.2009

Taugher, R.J., Y. Lu, R. Fan, A. Ghobbeh, C.J. Kreple, F.M. Faraci, and J.A. Wemmie. 2017. ASIC1A in neurons is critical for fear-related behaviors. *Genes Brain Behav.* 16:745–755. https://doi.org/10.1111/gbb.12398

Ugawa, S., T. Ueda, Y. Minami, M. Horimoto, and S. Shimada. 2001. A single amino acid substitution in MDEG2 specifically alters desensitization of the proton-activated cation current. *Neuroreport.* 12:2141–2145. https://doi.org/10.1097/00001756-200107200-00020

Vullo, S., G. Bonifacio, S. Roy, N. Johner, S. Bernèche, and S. Kellenberger. 2017. Conformational dynamics and role of the acidic pocket in ASIC pH-dependent gating. *Proc. Natl. Acad. Sci. USA.* 114:3768–3773. https://doi.org/10.1073/pnas.1620560114

Waldmann, R., G. Champigny, N. Voilley, I. Lauritzen, and M. Lazdunski. 1996. The mammalian degenerin MDEG, an amiloride-sensitive cation channel activated by mutations causing neurodegeneration in Caenorhabditis elegans. *J. Biol. Chem.* 271:10433–10436. https://doi.org/10.1074/jbc.271.18.10433

Wemmie, J.A., J. Chen, C.C. Askwith, A.M. Hruska-Hageman, M.P. Price, B.C. Nolan, P.G. Yoder, E. Lamani, T. Hoshi, J.H. Freeman Jr., and M.J. Welsh. 2002. The acid-activated ion channel ASIC contributes to synaptic plasticity, learning, and memory. *Neuron.* 34:463–477. https://doi.org/10.1016/S0896-6273(02)00661-X

Wu, Y., Z. Chen, and C.M. Canessa. 2019. A valve-like mechanism controls desensitization of functional mammalian isoforms of acid-sensing ion channels. *eLife.* 8:e45851. https://doi.org/10.7554/eLife.45851

Yoder, N., and E. Gouaux. 2018. Divalent cation and chloride ion sites of chicken acid sensing ion channel 1a elucidated by x-ray crystallography. *PLoS One.* 13:e0202134. https://doi.org/10.1371/journal.pone.0202134

Yoder, N., and E. Gouaux. 2020. The His-Gly motif of acid-sensing ion channels resides in a reentrant 'loop' implicated in gating and ion selectivity. *eLife.* 9:e56527. https://doi.org/10.7554/eLife.56527

Yoder, N., C. Yoshioka, and E. Gouaux. 2018. Gating mechanisms of acid-sensing ion channels. *Nature.* 555:397–401. https://doi.org/10.1038/nature25782

Zhang, P., and C.M. Canessa. 2002. Single channel properties of rat acid-sensitive ion channel-1α, -2a, and -3 expressed in Xenopus oocytes. *J. Gen. Physiol.* 120:553–566. https://doi.org/10.1085/jgp.20028574
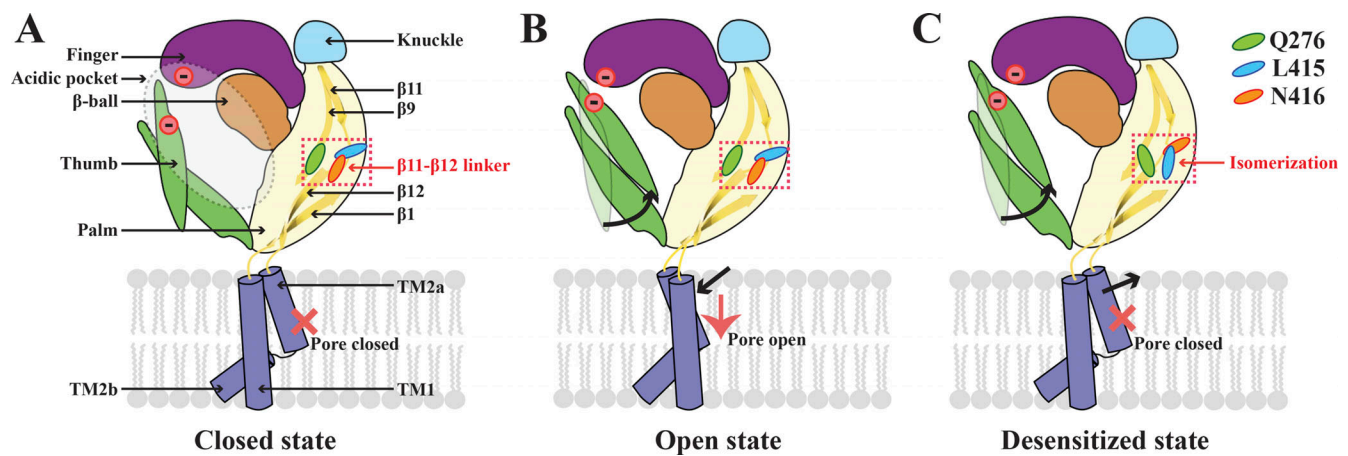
Figure S1. **Cartoon of putative β11-β12 desensitization mechanism.** A single subunit of the channel trimer is shown in closed, open, and desensitized conformations based on the corresponding structures of cASIC. The ECD is divided in subdomains marked by different colors. The acidic pocket is delineated by a dashed oval and encompasses negatively charged residues located in the thumb, finger, and palm. Residues L415 and N416 in the β11-β12 linker together with Q276 in the adjacent β9 strand are shown inside the orange square. **(A)** Closed or resting conformation (PDB accession no. 5WKV) with a relaxed thumb and expanded acidic pocket, and the side chain of N416 facing the interior of the lower palm. **(B)** Open conformation (PDB accession no. 4NTW). Here, the acidic pocket is collapsed owing to displacement of the α5-helix of the thumb, the lower palm is expanded, and the upper part of pore is also expanded, removing the constriction of the gate. **(C)** The desensitized state. The acidic pocket remains collapsed, the lower palm is contracted, residues L415 and N416 in the β11-β12 linker have undergone isomerization (180° flipping), and the transmembrane domain narrows, shutting the pore. Structures of cASIC in SSD (PDB accession no. 6VTK) and desensitized by low pH are almost identical (PDB accession no. 3IJ4).
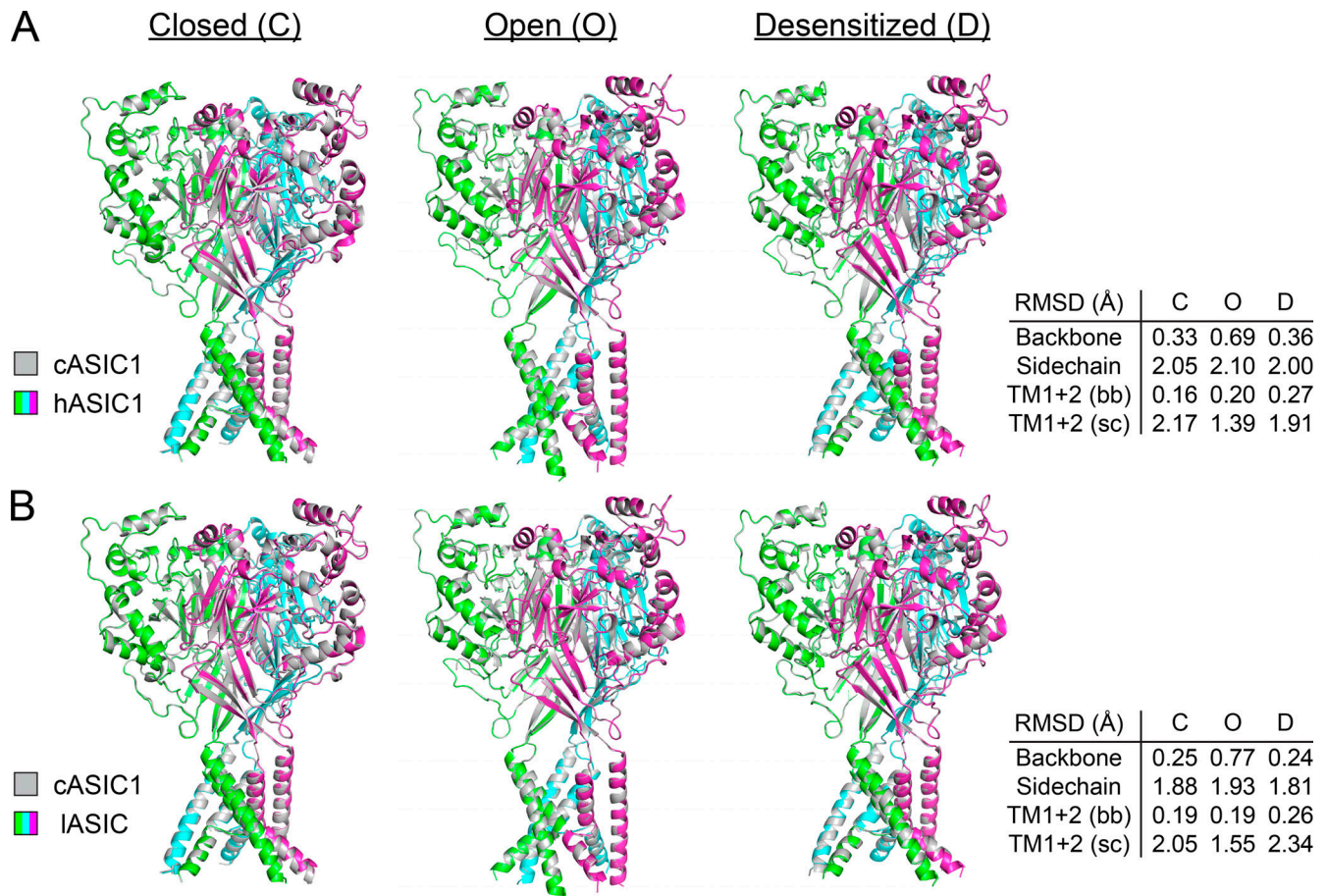
Figure S2. **Comparison of Rosetta homology models of ASIC channels with experimental structures of cASIC1. (A and B)** Homology models of hASIC1 (A) and lASIC (B) are compared with crystal structures of cASIC1 in closed (PDB accession no. 5WKV), open (PDB accession no. 4NTW), and desensitized (PDB accession no. 4NYK) conformations. The root-mean-squared distance (RMSD) deviations between all backbone (bb) or side chain (sc) heavy atoms resulting from the structural alignments in A and B are shown next to the structural models.

Chen et al.
Arginine 64 sets stability of open and closed states in ASIC

Journal of General Physiology   S2
https://doi.org/10.1085/jgp.202012802
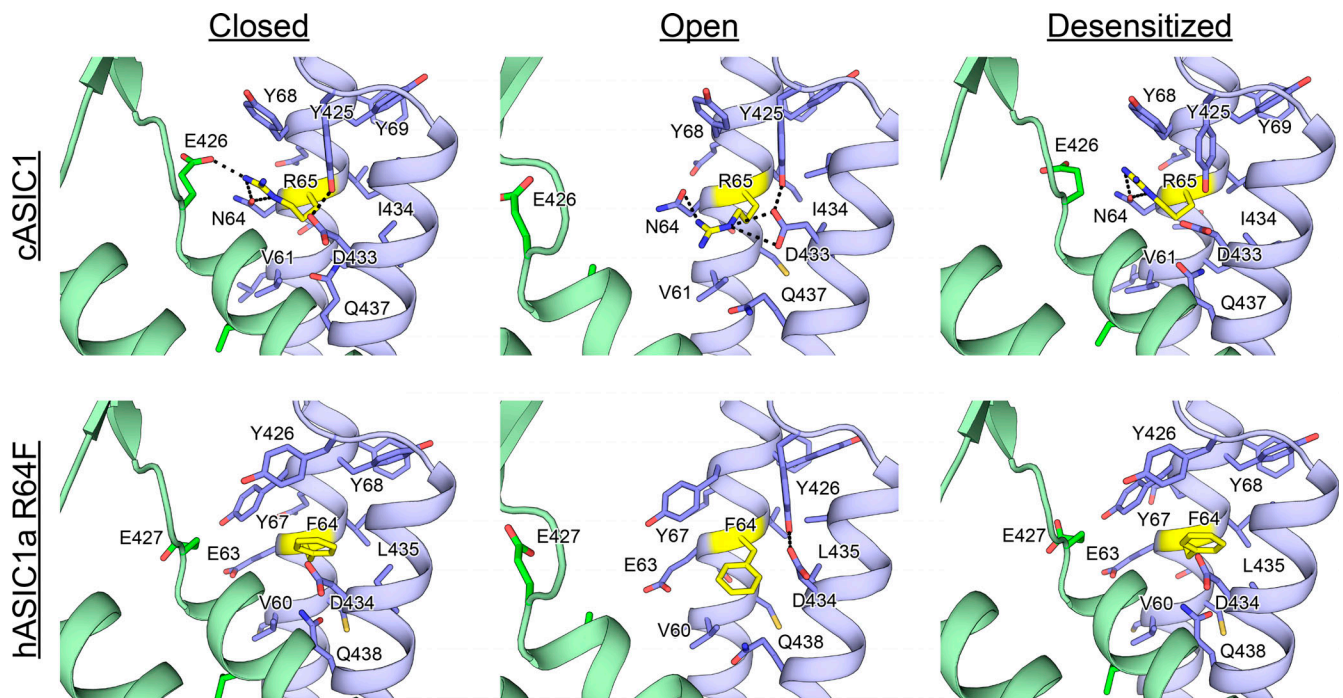
Figure S3. **Cartoon representations of x ray–determined structures of cASIC1a- and Rosetta-predicted models of hASIC1a R64F. (A)** Residue neighborhood around R65 (yellow) in the closed (PDB accession no. 5WKV), open (PDB accession no. 4NTW), and desensitized (PDB accession no. 4NYK) state structures of cASIC1a. The TM segments of two cASIC1a subunits are depicted as ribbons and colored blue and green, respectively. The third subunit is not shown for clarity. Residue side chains are depicted as sticks, and polar contacts are indicated as dashed lines. **(B)** Residue neighborhood around the substituted residue F64 (yellow) in Rosetta models of the closed, open, and desensitized state structures of hASIC1a-R64F.
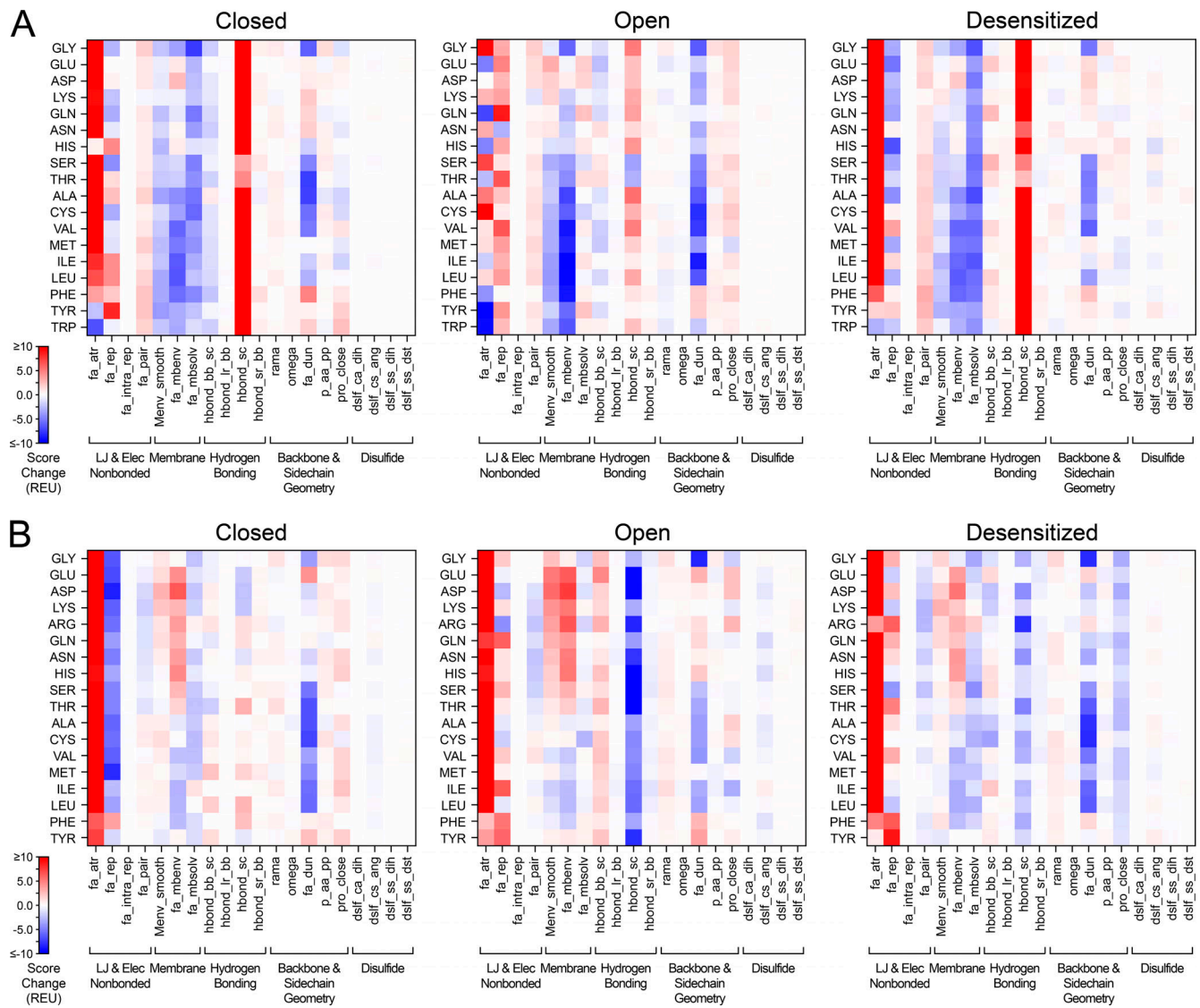
Figure S4. **Breakdown of computationally predicted protein stability changes for hASIC1a-R64 and lASIC-W66 mutants by Rosetta score term. (A and B)** For every amino acid substitution at residue 64 in hASIC1a (A) or residue 66 in lASIC (B), the contributions of the individual score terms in the RosettaMembrane energy function to the stability change of the closed, open, and desensitized state structure, respectively, are shown. LJ, Lennard-Jones; Elec., electrostatic interaction energy.

Chen et al.
Arginine 64 sets stability of open and closed states in ASIC

Journal of General Physiology   S4
https://doi.org/10.1085/jgp.202012802
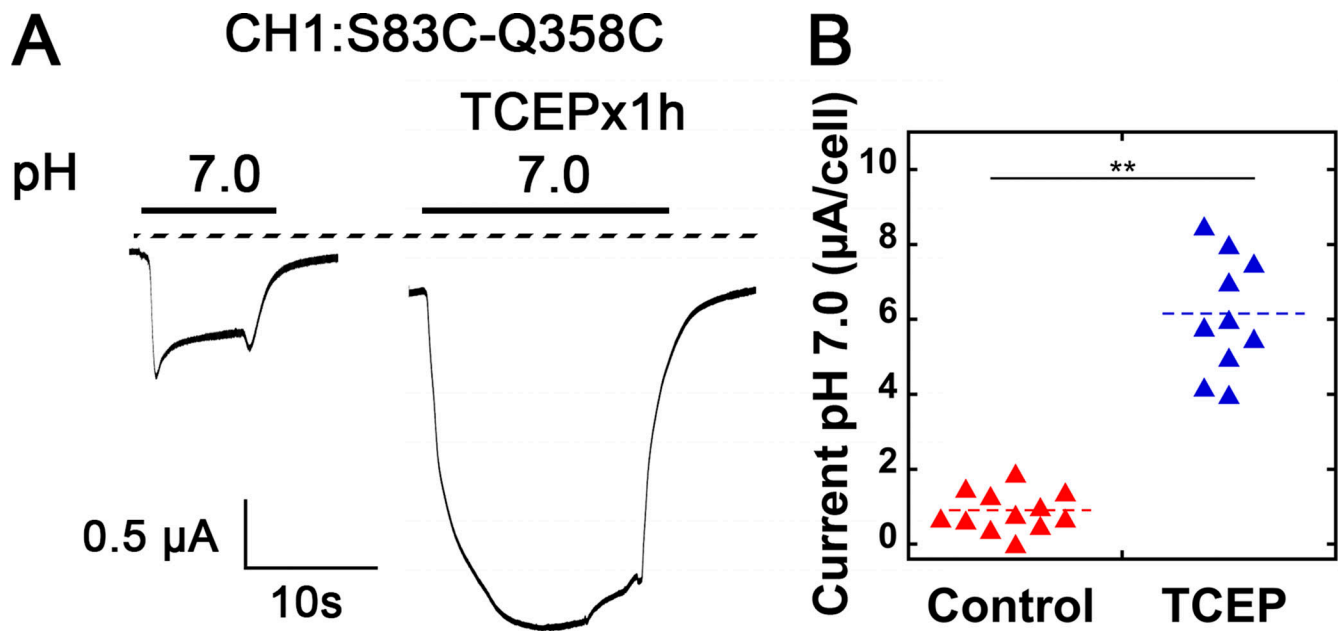
Figure S5. **Effect of a reducing agent on the activity of S83C-Q358C CH1. (A)** Representative example of whole cell currents from cells expressing CH1: P85C-Q358C channels activated with pH 7.0 before and after treatment with the reducing agent TCEP for 1 h. **(B)** Summary of current values of before (n = 12) and after treatment (n = 10) with TCEP reducing agent. Two oocytes were damaged and not included in the TCEP results. Asterisks indicate statistically significant difference between the two groups by t test; **, P < 0.001.